Inorganic Chemistry

pubs.acs.org/IC
Article

Generation of $[(N4Py)Fe(IV){=}O]^{2+}$ through Heterolytic O−O Bond Cleavage in $[(N4Py)Fe(II)(OOH)]^{+}$

Juan Chen, Andy S. Sardjan, C. Maurits de Roo, Marika Di Berto Mancini, Apparao Draksharapu, Davide Angelone, Ronald Hage, Marcel Swart,* and Wesley R. Browne*

Cite This: *Inorg. Chem.* 2025, 64, 9408−9417

ABSTRACT: High-valent Fe(IV) oxido species are important intermediates in the catalyzed oxidation of organic compounds by nonheme iron enzymes. These species can be generated in biomimetic model complexes directly using oxygen atom transfer oxidants, e.g., PhIO and ClO^-. Their formation by heterolysis of the O−O bond of putative Fe(II)-OOH species (formed from Fe(II) precursors and H_2O_2) has scarcely been observed. Reaction with near-stoichiometric H_2O_2 typically shows initial formation of Fe(III)-OH and Fe(III)-OOH species, with homolytic O−O bond cleavage thereafter proposed to generate the Fe(IV)═O state. Here, we show that $[(N4Py)Fe(IV){=}O]^{2+}$ (where N4Py = 1,1-di(pyridin-2-yl)-*N*,*N*-bis(pyridin-2-ylmethyl)methanamine) is formed with substoichiometric H_2O_2 in methanol through heterolytic cleavage of the O−O bond of an Fe(II)-OOH intermediate. Temperature-dependent studies show that the ligand exchange reactions preceding formation of the Fe(II)-OOH species and subsequent comproportionations limit the yield of the Fe(IV)═O species. Furthermore, comproportionation proceeds through hydrogen atom transfer from $[(N4Py)Fe(II)(OH_2)]^{2+}$ to $[(N4Py)Fe(IV){=}O]^{2+}$. These data rationalize the extent of the initial conversion of $[(N4Py)Fe(II)(CH_3CN)]^{2+}$ to $[(N4Py)Fe(IV){=}O]^{2+}$ under conditions relevant to catalytic oxidations. The heterolytic pathway to formation of $[(N4Py)Fe(IV){=}O]^{2+}$ is a key step in the development of iron(II) oxidation catalysts that can cycle between the Fe(II) and Fe(IV)═O states, avoiding nonselective reactive oxygen species.

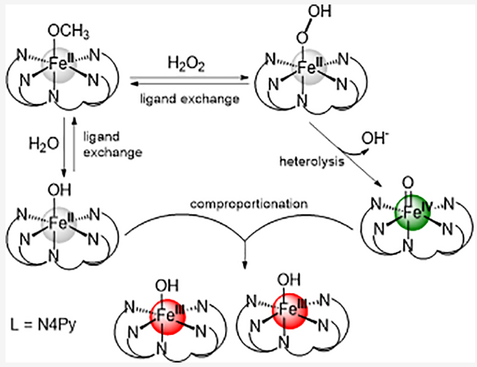

INTRODUCTION

High-valent Fe(IV)═O species are invoked frequently as the reactive species in the oxidation of organic substrates by heme and nonheme enzymes.[1−3] In nature, enzymes use O_2 and electron donors to generate these species from the Fe(II) redox state, e.g., through electron transfer chains or oxidative decarboxylation. Biomimetic nonheme Fe(IV)═O species have been generated from the corresponding Fe^{II} complexes of tetradentate N4 (TMC (tetramethylcyclam), BPMCN (*N*,*N*-bis(2-pyridylmethyl)-*N*,*N*-dimethyl-trans-1,2-diaminocyclohexane), etc.) and pentadentate N5 (N4Py, Bn-TPEN (N-benzyl-*N*,*N*′*N*′-tris(2-pyridylmethyl)-1,2-diaminoethane), bispidine, etc.) ligands,[4] using two-electron oxidants, such as *m*-CPBA and peracetic acid,[5,6] PhIO,[7−9] HOCl,[10] and hydroperoxides (e.g., *tert*-butyl-hydroperoxide and H_2O_2).[7,11−16] In these catalysts, typically rapid net oxidation to an Fe^{III} (resting) state is observed with H_2O_2, and the relatively stable Fe^{III} (hydro)peroxy species is the starting point in catalytic cycles, not least because an Fe(III)-OOH species is observed in many cases.[14,17,18] Indeed, it is the last observed intermediate in the cleavage of DNA with O_2 by the antibiotic, iron bleomycin.[19] O−O bond homolysis of the Fe(III)-OOH species to yield an Fe(IV)═O species and a hydroxyl radical is generally assumed, although, more recently O−O bond heterolysis to form a Fe(V)═O species has been proposed.[20−26] The initial reaction between the Fe(II) complexes and H_2O_2, however, can be slow in solvents such as acetonitrile. Recently, McKenzie and Que groups have shown that including carboxylato motifs in the ligand makes the Fe(III) oxidation state the most stable form in solvents such as acetonitrile, which facilitates their reactions with oxidants.[27−31] Catalytic pathways that involve only an Fe^{II}/Fe^{IV} redox cycle are involved less often, despite the finding that the rebound mechanism,[32] invoked often in C−H oxidation by Fe(IV)═O species, recovers the Fe(II) oxidation state. Chemical reduction of Fe(III)-OOH complexes and stoichiometric reactions between nonheme Fe^{II} complexes and H_2O_2 have received some attention, most notably by Nam,[33,34] and by Que, Hirao, Comba, Banse, and co-workers, respectively.[35−39] Under basic conditions at −40 °C, the N4-coordinated $[(TMC)Fe^{II}]^{2+}$ complex (Figure 1) provides the correspond-

Received: December 3, 2024
Revised: April 3, 2025
Accepted: April 10, 2025
Published: May 2, 2025

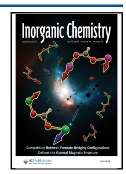

https://doi.org/10.1021/acs.inorgchem.4c05172
Inorg. Chem. 2025, 64, 9408−9417

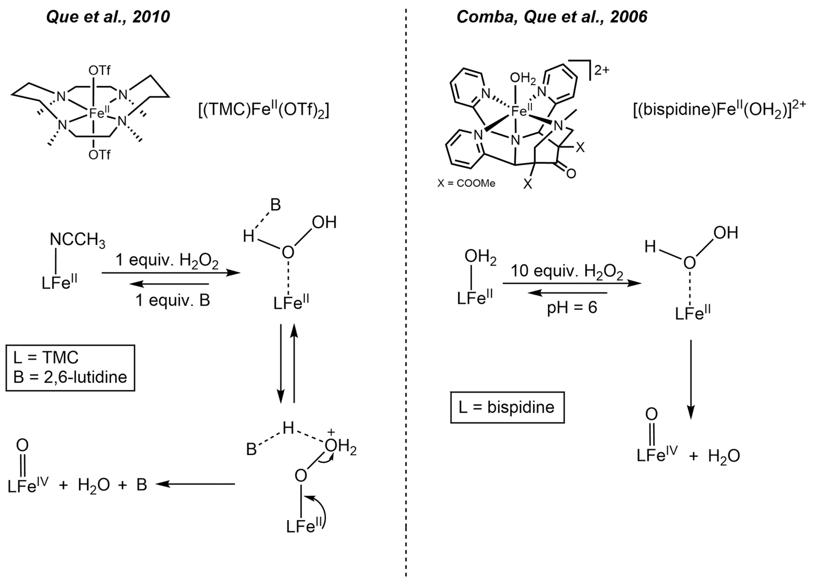

Figure 1. Fe(II) complexes discussed and the formation of Fe(IV)═O species through O−O bond heterolysis reported earlier.

ing Fe(IV)═O species directly in over 90% yield with sub- and near-stoichiometric H_2O_2.[35] Intramolecular base-promoted heterolysis was observed during the reaction of $[(^{NH}Bn\text{-}TPEN)Fe^{II}]^{2+}$ with H_2O_2 in which a pendant base (an alkylamine) was introduced into the second coordination sphere to facilitate a proton-transfer-driven heterolytic O−O bond cleavage step.[35,36,38] The quantitative generation of an Fe(IV)═O species from Fe^{II} complexes is not reported in other N4 and N5 systems; however, for the N5-coordinated Fe^{II}(bispidine) complex (Figure 1), an Fe(IV)═O species was formed in water upon reaction with H_2O_2 in up to 60% yield.[36] The lack of quantitative conversion in the latter case may be due to competing reactions, in particular, comproportionation between the Fe^{II} precursor and the Fe(IV)═O species generated, or reaction of H_2O_2 with the Fe(IV)═O species formed.[40] Nevertheless, these studies show that the generation of Fe(IV)═O species in a Fe^{II}/Fe^{IV} cycle is feasible.

Conditions in which Fe(IV)═O species form by O−O bond heterolysis in Fe(II)-OOH species is of fundamental interest since this pathway avoids the hydroxyl radicals that accompany O−O bond homolysis in Fe(III)-OOH species.[32,41]

The complex $[(N4Py)Fe(II)(NCCH_3)](ClO_4)_2$ (**1**), bearing an N5 ligand, reacts with excess H_2O_2 in acetonitrile, forming a relatively stable Fe(III)-OOH intermediate, which was proposed to generate an Fe(IV)═O species upon homolytic cleavage of the O−O bond.[17,18,42] Although the Fe(IV)═O species ($[(N4Py)Fe(IV)\!=\!O]^{2+}$, **4**) is also relatively stable (can be isolated),[4,8] its formation from the Fe(III)-OOH species is not readily observed, and its absence under reaction conditions with H_2O_2 is expected considering that it reacts rapidly with H_2O_2 to form Fe(III)-OH and $O_2^{\bullet-}$.[43] However, our recent studies in methanol show that the rate of cleavage of the O−O bond of Fe(III)-OOH is unexpectedly low and does not compete with H_2O_2 disproportionation by Fe(III)-OOH, nor with the reaction between two molecules of Fe(III)-OOH.[44]

Heterolytic O−O bond cleavage in an initially formed Fe(II)-OOH species would yield the same Fe(IV)═O species; however, the rapid reaction between Fe(IV)═O and H_2O_2, as well as the comproportionation reaction between Fe^{II} and Fe(IV)═O species can be expected to preclude the observation of **4**. In acetonitrile, **1** shows little if any reaction with stoichiometric H_2O_2, and only slow oxidation to the Fe(III) state is observed with excess (>50 equiv) H_2O_2.[40,43]

The low reaction rate is due to the kinetic and thermodynamic inertness of the low-spin CH_3CN-bound Fe(II) complex. Exchange of the CH_3CN ligand, ultimately with H_2O_2, is required for oxidation of the complex to take place; however, ligand exchange is unfavorable, even with excess H_2O_2. Hence, the initial reaction of H_2O_2 with the N5 Fe(II) complexes to form a putative Fe(II)-OOH precursor or Fe(IV)═O species is too slow, compared to subsequent reactions, to allow for a buildup in the concentration of either species in CH_3CN.

In methanol, exchange of the acetonitrile ligand of **1** with methanol is immediate (from **1** to **2a**, Scheme 1).[43,45] A preference for the sixth ligand for [(N4Py)Fe(II)] follows the

Scheme 1. Reactions Following the Addition of Stoichiometric H_2O_2 to 1 in Methanol[a]

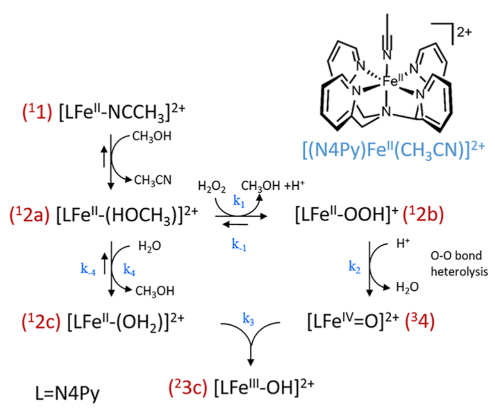

[a]Note that in the Fe(II) oxidation state, the coordination of the solvent (CH_3OH and H_2O), as shown for **2a** and **2c**, is favored thermodynamically, while in the Fe(III) oxidation state, the CH_3O^- and HO^- bound complexes are lower in energy, based on DFT calculated energies; vide infra.

order $CH_3CN \gg H_2O > HOCH_3$, and hence displacement of aquo and methanol/methoxido ligands by H_2O_2 is rapid, in contrast to the rate of exchange in acetonitrile.[45]

In this contribution, we make use of the higher rates of ligand exchange in methanol compared to those in acetonitrile to demonstrate that heterolytic cleavage of the O−O bond of a putative Fe(II)-OOH species (**2b**) generates an Fe(IV)═O species (**4**) directly. The influence of potential side reactions, for example, comproportionation between Fe(IV)═O and Fe(II), spin-crossover/ligand exchange of the Fe(II) complex at various temperatures, and reaction of Fe(IV)═O with H_2O_2, is evaluated through experiments and quantum chemical calculations. We show that the temperature dependence of the equilibria between acetonitrile, water, and methanol as the sixth ligand in **1** has a decisive impact on the species observed and, therefore, the catalytic reactivity of **1** with H_2O_2 that can be expected.

■ RESULTS AND DISCUSSION

The extent to which the Fe(II) species can be oxidized to the Fe(IV)═O state, rather than the Fe(III) state, depends on the rates of ligand exchange between the solvent and H_2O_2, as well as other reactions such as comproportionation. Hence, the temperature dependence of speciation in methanol is established before exploring reactions with H_2O_2.

Speciation of 1 in Methanol. The differences in redox potentials[45] and stability calculated by DFT methods (*vide infra*) indicate that **1** is thermodynamically more stable than its $H_2O/HO^-/MeOH/MeO^-$ bound [(N4Py)Fe(II)] analogues, e.g., **2a**. However, the exchange of the CH_3CN ligand in **1** for methanol and water occurs immediately upon dissolution in either solvent manifested in changes in UV/vis absorption, cyclic voltammetry, and ESI mass spectrometry.[43] Addition of 1 vol% (0.25 M) acetonitrile to methanol is sufficient to see an almost complete recovery of the visible absorption spectrum of **1** (Figure S1), i.e., an increase in molar absorptivity of the ^{1}MLCT absorption band due to exchange of the methanol ligand with CH_3CN. One vol% amount of water is sufficient to decrease the visible absorbance in methanol due to exchange of the methanol ligand with H_2O (Figure S2). These effects highlight the fine balance between the various Fe(II) species in solution and the relatively rapid interconversion between them (Scheme 2).

Scheme 2. Ligand Exchange Reactions of 1 in Methanol

$$\underset{(^1\mathbf{1})}{[LFe^{II}\text{-}NCCH_3]^{2+}} \underset{1\ \text{vol\%}\ CH_3CN}{\overset{CH_3OH}{\rightleftharpoons}} \underset{(^1\mathbf{2a})}{[LFe^{II}\text{-}(HOCH_3)]^{2+}} \overset{1\ \text{vol\%}\ H_2O}{\rightleftharpoons} \underset{(^1\mathbf{2c})}{[LFe^{II}\text{-}(OH_2)]^{2+}}$$

Consistent with this, the UV/vis absorption spectrum of **1** in methanol shows a strong temperature dependence (Figure S3). As the temperature is decreased to −30 °C, the characteristic visible absorption band of **1** recovers almost completely and is lost reversibly as the temperature is raised to 30 °C. These changes are consistent with a interconversion between the high-spin **2a** and low-spin **1**. Hence, ligand exchange is temperature-dependent in methanol: at room temperature, **2a** is the most abundant complex in solution, while at low temperature it is **1**. The assignment of these temperature-dependent changes in the 6th ligand is confirmed by the absence of temperature dependence in the UV/vis absorption spectrum of **2a**, formed by mixing the ligand N4Py with $Fe(II)SO_4$ in methanol (i.e., without CH_3CN) (Figure S4). Taken together, the data indicate that at the concentrations of **1** used in the present study, i.e., between 0.25 and 1 mM in methanol, at room temperature, ca. 15% of the Fe(II) complex is present as **1** and 85% as **2a**.

Reaction with Near-Stoichiometric H_2O_2. Addition of stoichiometric amounts of H_2O_2 to **1** in acetonitrile does not significantly affect its UV/vis absorption spectrum (i.e., <1% of the complex is oxidized to the Fe(III) state) despite that the H_2O_2 is consumed (Figure S5). The exchange of the CH_3CN ligand of **1** with the solvent in methanol and water reduces the barrier to ligand exchange with, e.g., H_2O_2, and hence the reaction of **1** with stoichiometric H_2O_2 in methanol is faster and proceeds to the Fe(III) state to a greater extent than in CH_3CN.

Accordingly, the addition of H_2O_2 in a stepwise manner to **1** in methanol shows a stepwise decrease (20% per step, Figure 2) in absorbance (350−500 nm), corresponding to the net oxidation of the Fe(II) complex to the Fe(III) state. A stepwise appearance of a weak absorption band at 692 nm accompanies the decrease. This absorption band is characteristic of $[(N4Py)Fe(IV){=}O]^{2+}$ (**4**). The extent of formation is up to 12% yield of **4** w.r.t. H_2O_2 added (Figure 2). UV/vis absorption spectroscopy shows complete oxidation of **1** to, eventually, $[(N4Py)Fe(III)(OCH_3)]^{2+}$ (**3a**), consistent with the expected 2:1 stoichiometry (**1**:H_2O_2), indicating relatively little loss of H_2O_2 due to disproportionation under these conditions.[43] X-band EPR spectroscopy ($S = \frac{1}{2}$ signal at g = 2.29, 2.12, and 1.96; see Figure S6) and resonance Raman spectroscopy (Figure S7) show that the major product is **3a**. Resonance Raman spectroscopy (λ_{exc} 355 nm, Figure S7) shows the appearance of the Fe(III)-OCH_3 stretching band at 554 cm^{-1}, the intensity of which increases with the addition of each 0.1 equiv of H_2O_2 (up to 0.6 equiv). This band is assigned to ν_{str} Fe-OCH_3 based on the shift from 554 to 531 cm^{-1} ($\Delta\tilde{\nu}$ = 23 cm^{-1}) in CD_3OD (a shift with CH_3OD is not observed) and the DFT calculated frequency (585 cm^{-1}) and corresponding shift (22 cm^{-1}) for $[(N4Py)Fe(III)(OCH_3)]^{2+}$ to $[(N4Py)Fe(III)(OCD_3)]^{2+}$ (Figure S8). Resonance enhancement of the band at 355 nm is consistent with a ligand-to-metal charge transfer transition, and the Fe-OCH_3 vibration is close to the same band in the Fe(III)-OCH_3 form of Bleomycin (530 cm^{-1}).[46] The efficiency in the oxidant suggests that the reaction of H_2O_2 with **2a** is faster than with **4** or **3a**.

The <12% yield of Fe(IV)═O obtained with a 2:1 ratio of **1**:H_2O_2 in the present study is much less efficient than that obtained earlier with $[(TMC)Fe^{II}]/H_2O_2$ (1:1 ratio) and $[Fe^{II}(bispidine)]/H_2O_2$ (>1:1) systems.[35,36] The minor amounts of **4** (Figure 3) obtained could arise either by O−O bond homolysis in an Fe(III)-OOH intermediate (eq 1), as proposed for Fe^{II}(bispidine) in methanol (vide supra),[36,46] or upon O−O bond heterolysis in an Fe(II)-OOH species formed initially (**2b**) (eq 2)

$$[(N4Py)Fe^{III}-OOH]^{2+} \xrightarrow{\text{homolytic cleavage}} [(N4Py)Fe^{IV}=O]^{2+} + HO^{\bullet} \quad (1)$$

$$[(N4Py)Fe^{II}-OOH]^{+} \xrightarrow{\text{heterolytic cleavage}} [(N4Py)Fe^{IV}=O]^{2+} + HO^{-} \quad (2)$$

https://doi.org/10.1021/acs.inorgchem.4c05172
Inorg. Chem. 2025, 64, 9408−9417

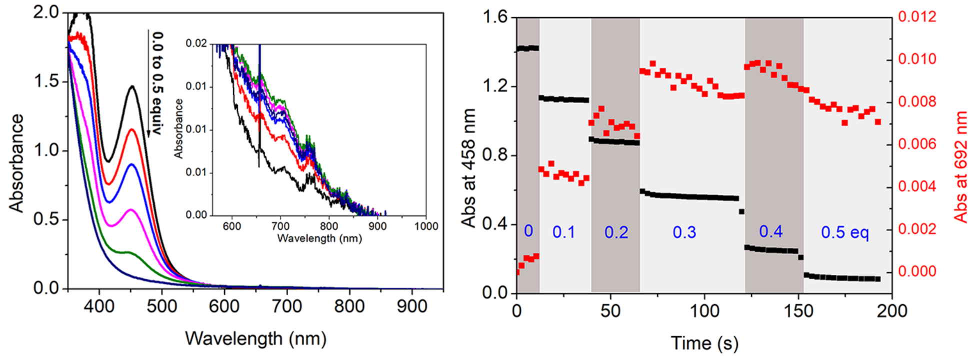

Figure 2. Addition of H_2O_2 (50% v/v in H_2O) in 0.1 equiv increments to **1** (0.5 mM) in CH_3OH at 21 °C. (left) UV/vis absorption spectra (black: initial, red: 0.1 equiv, blue: 0.2 equiv, magenta: 0.3 equiv, green: 0.4 equiv, navy: 0.5 equiv) with the NIR region shown as an inset. (right) Changes in absorbance at 458 nm (Fe(II), black) and 692 nm (Fe(IV)=O, red).

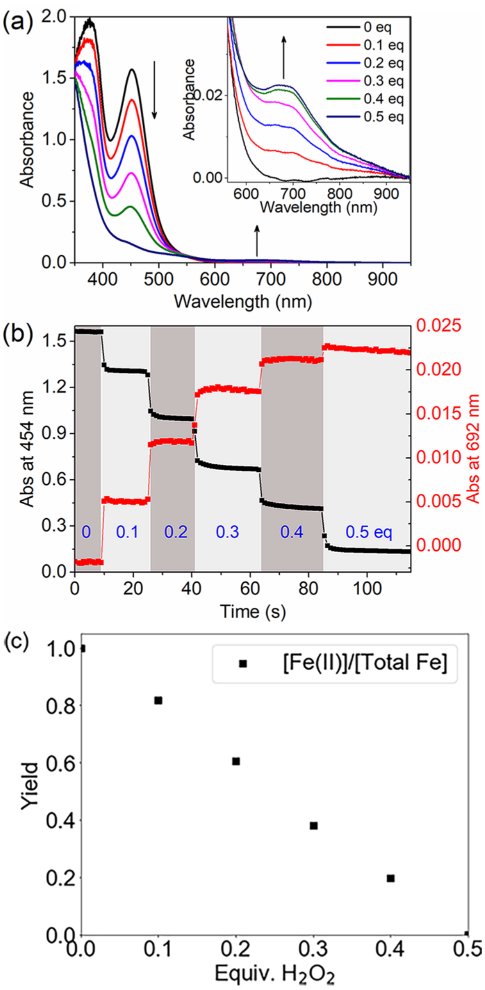

Figure 3. (a) Addition of H_2O_2 in steps to **1** (0.5 mM) in CD_3OD at 21 °C. UV/vis absorption spectra; initial (black) and at 0.1 (red), 0.2 (blue), 0.3 (magenta), 0.4 (green), and 0.5 (navy) equiv H_2O_2. Inset: 560−950 nm region. (b) Change in abs. at 454 nm (Fe(II), black) and 692 nm (Fe(IV)=O, red). (c) Extent of oxidation of **1** with respect to the total concentration of iron during stepwise addition of H_2O_2 in CD_3OD.

The homolytic pathway (eq 1) can be excluded since the rate at which it proceeds was shown earlier to be 2.2×10^{-4} s^{-1} in methanol and is not a kinetically competent pathway on the time scale of oxidations here (within seconds).[43,44] Indeed, addition of excess H_2O_2 (50 equiv) to Fe(III)-OCH_3 (Figure S9) results in the appearance of the characteristic absorption band of Fe(III)-OOH (λ_{max} 550 nm). Its subsequent decay is slow (3.0×10^{-4} s^{-1})[43] and contrasts with the instantaneous formation of **4** upon the addition of H_2O_2 to **1** (Figures 2 and 3). Furthermore, the barrier to the O−O bond homolysis in $[(N4Py)Fe(III)(OOH)]^{2+}$ is estimated by DFT to be +19.1 kcal mol^{-1}.[47] Hence, both data reported earlier and in the present report (experimental and calculated) exclude the homolytic pathway from Fe(III)-OOH. The overall 2:1 stoichiometry is consistent with heterolytic O−O bond cleavage in a putative Fe(II)-OOH (eq 2) species, which, according to DFT calculations, is highly exergonic (*vide infra*, Scheme 3). Complex **4** can engage in the oxidation of both

Scheme 3. Gibbs Free-Energy Changes (S12g/TZ2P//BP86-D$_3$/TDZP) for the Proposed Mechanism

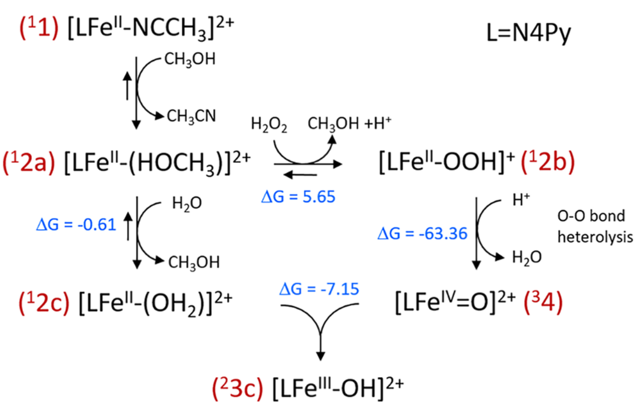

alcohol (solvent oxidation) and H_2O_2 through HAT,[40,48] as well as comproportionation with **2c** in methanol. The subsequent comproportionation between the Fe(IV)=O species and Fe(II)-OCH_3/H_2O complexes, as shown earlier in H_2O, can account for the essentially stoichiometric oxidation with the two-electron oxidant H_2O_2.[10] These processes complicate the kinetic analysis of the reaction of **1** with H_2O_2. The availability of **4** prepared independently[10] allows for the relative kinetic competence of various reactions to be established.

Comproportionation and Solvent Kinetic Isotope Effects. Comproportionation between **1** and independently prepared **4** proceeds with the visible absorption band of **1** decreasing concomitant with the NIR absorption band of **4**

https://doi.org/10.1021/acs.inorgchem.4c05172
Inorg. Chem. 2025, 64, 9408−9417

(Figure 4). The rate of comproportionation ($k_{obs} > 6.0 \times 10^{-3}$ s^{-1}, Table S1) is three times that of the oxidation of methanol to formaldehyde by **4** (Figure S10; 1.8×10^{-3} s^{-1}, Table S1).[49] Indeed, formaldehyde was not detected in significant amounts following comproportionation.[50] The final product, $[(N4Py)Fe(III)(OCH_3)]^{2+}$, was corroborated by resonance Raman and EPR spectroscopy (Figure S11).

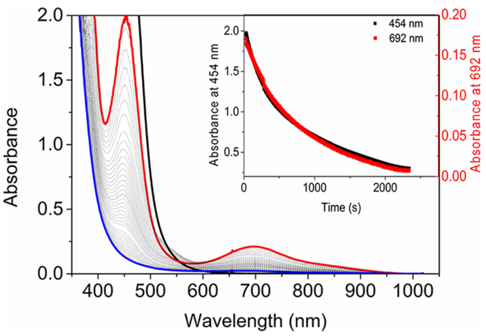

Figure 4. UV/vis absorption spectrum of **1** (1 mM in methanol) before (black line) and 5 s after (red line) the addition of an equimolar/volume solution of **4**; final analytical concentrations of **1** and **4** were 0.5 mM each; final spectrum shown in blue. Inset: Changes in absorbance at 454 nm due to Fe(II) and at 692 nm due to Fe(IV)═O over time.

Comproportionation is slower in CD_3OD ($k_{obs} = 1.3 \times 10^{-3}$ s^{-1}, Table S1, apparent KIE = 4.6) but is still 20 times faster than the rate of oxidation of CD_3OD by **4**. Notably, the rate of comproportionation increases upon the addition of H_2O (Figure S12), which indicates that an inner sphere mechanism for electron transfer (e.g., HAT) between **2c** and **4** occurs rather than between **4** and **2a**. It should be noted that H_2O_2 is added as a (50 wt%) solution in water. Addition of excess H_2O_2 will also result in the addition of excess H_2O, accelerating comproportionation.

Comproportionation of **1** with **4** in H_2O was reported[10] earlier and in the present study (Figure S1), and the reaction in H_2O ($k_{obs} = 1.12$ s^{-1}, Figure S13) is over 1000 times faster than in methanol but nevertheless still shows a KIE of ca. 3 (in D_2O, $k_{obs} = 0.4$ s^{-1}, Figure S1). These data support that comproportionation is between **4** and **2c** and that the KIE observed in CH_3OH is due to rapid H/D equilibration between methanol and water. The conclusion that **2c**, and not **2a**, reacts with **4** is further supported by the observation that in methanol at −30 °C, comproportionation does not occur due to the recovery of the CH_3CN-bound complex **1** at that temperature (*vide supra*). The absorption bands for both **1** and **4** do not change until 10 vol% H_2O ($k_{obs} = 3.9 \times 10^{-3}$ s^{-1}, Table S1) has been added, and the rate of change increases further with 50 vol% H_2O added ($k_{obs} = 4.3 \times 10^{-2}$ s^{-1}, Table S1, Figure S14).

The data indicate that conversion of **1** to the final Fe(III) species proceeds through ligand exchange, from **2a** to **2b** (Fe(II)-$HOCH_3$ to Fe(II)-OOH), followed by O−O bond heterolysis to form **4** and OH^- (within the mixing time, <1 s). The formed Fe(IV)═O then comproportionates with $[(N4Py)Fe(II)(OH_2)]^{2+}$ (**2c**) to generate $[(N4Py)Fe(III)(X)]^{2+}$ (X = OH or OCH_3, Scheme 1). Therefore, the 2:1 stoichiometry (**1**:H_2O_2) seen in the conversion of **1** to an Fe(III) species is mainly due to equilibration of **2a** in methanol with adventitious H_2O, and with H_2O_2.

This mechanism predicts that the concentration of **4** will build up significantly in methanol due to its slow reaction with the methanol-bound Fe(II) complex (**2a**). Solvent deuteration (KIE = 4) retards comproportionation sufficiently to allow for a higher concentration of **4** to accumulate (Figure 3). In methanol, the reaction of H_2O_2 with **2a** is much faster (<1 s) than the reaction of H_2O_2 with **4** ($k_{obs} = 1.0 \times 10^{-2}$ s^{-1} in CH_3OH and 1.0×10^{-3} s^{-1} in CD_3OD),[43] and hence the latter reaction cannot compete, leading to a buildup of **4**. Furthermore, although **4** accumulates after each substoichiometric addition of H_2O_2, comproportionation with **2c** reduces the concentration of **4** again (Figure 3).

Impact of Temperature and Ligand Exchange Rates. A common approach to stabilizing reactive species is to generate them at a low temperature. At −30 °C in methanol, stepwise addition of H_2O_2 to **1** results in the concomitant stepwise decrease in visible absorbance due to oxidation to the Fe(III) state (Figure 5). In contrast to ambient conditions, complete oxidation requires >0.5 equiv H_2O_2. In addition, the absorbance in the NIR region does not increase, i.e., **4** does not accumulate. Only 66% of **2a** is oxidized to the Fe(III) state by the addition of 0.5 equiv H_2O_2, but the extent increases to 77 and >90% when 5 and 10 vol % H_2O is present, respectively (Figures S15 and S16).

With $[(N4Py)Fe(II)\text{-}HOCH_3]^{2+}$ instead of **1** (i.e., CH_3CN is not present even as a ligand), only 0.5 equiv of H_2O_2 is necessary for full oxidation of $[(N4Py)Fe(II)\text{-}HOCH_3]^{2+}$ in MeOH at −40 °C (Figure S17). Hence, without the CH_3CN ligand, exchange of the methanol ligand of [(N4Py)Fe(II)-

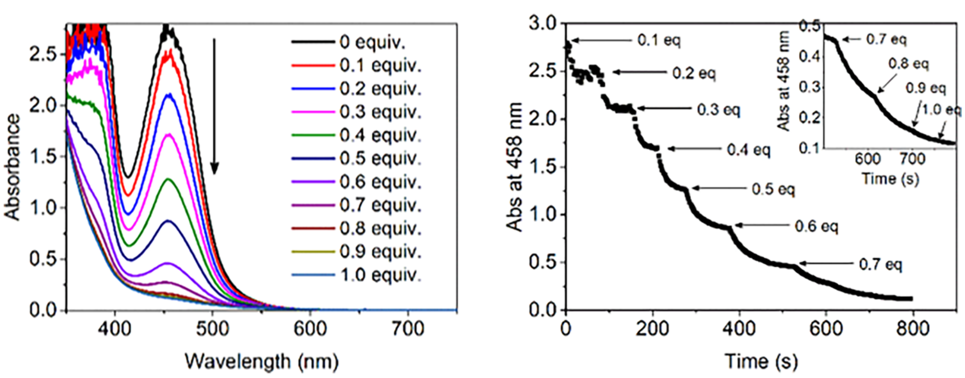

Figure 5. (Left) UV/vis absorption spectra of the addition of H_2O_2 in steps at −30 °C to **1** (0.5 mM) in CH_3OH. (Right) Changes in abs. at 458 nm for 0.7−1.0 equiv shown in detail in the inset.

https://doi.org/10.1021/acs.inorgchem.4c05172
Inorg. Chem. 2025, 64, 9408−9417

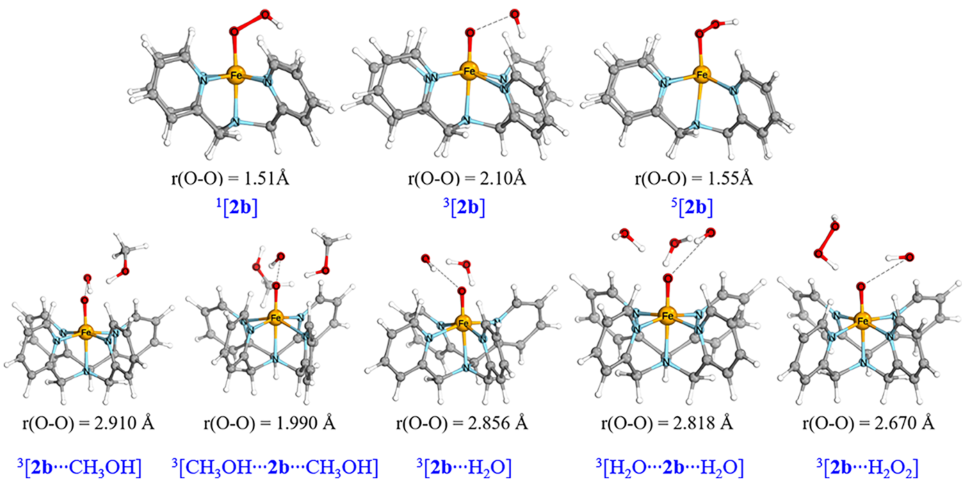

Figure 6. (Top) Optimized geometries (BP86-D$_3$/TDZP) for **2b** in different spin states. (Bottom) Corresponding optimized geometries of **2b** with S = 1 with various adducts, including one or two methanol molecules, one or two H_2O molecules, and a H_2O_2 molecule; only four representative structures are shown (the complete table is shown in Table S4).

$HOCH_3]^{2+}$ with H_2O_2 is sufficiently rapid for the oxidation of the Fe(II) complex to compete with other reactions. These data indicate that solvent exchange reactions are retarded sufficiently for the reaction of **4**, formed initially, with H_2O_2. In addition, disproportionation of H_2O_2 via a Fe(III)-OOH species can occur.[44]

The differences in behavior at low and ambient temperatures can be rationalized by consideration of the rates of each of the individual steps in the multistep reaction, together with the temperature-dependent equilibrium between **1** and **2a** in both methanol (Scheme 3) and H_2O (Figure S18). The singlet−quintet spin-state switching accompanying ligand exchange is manifested by a reversible change in the molar absorptivity of the MLCT bands at 380 and 454 nm as the temperature decreases and increases (Figure S19). At −30 °C (Table S1), both the oxidation of **2a** (1.0×10^{-2} s^{-1}, due to its low concentration), and comproportionation between **2c** and **4** (*vide supra*, Figure S14) are slower, and hence oxidation of **2a** via a comproportionation pathway is not significant. Hence, H_2O_2 is likely consumed by other processes, e.g., reaction with Fe(IV)═O and direct reaction between Fe(III)-OOH and H_2O_2 as shown earlier.[40,43] As is the case in CH_3CN at room temperature, in methanol at −30 °C, the CH_3CN/H_2O_2 ligand exchange (in **1**) is slow and is the rate-determining step. Hence, any **4** produced can react with H_2O_2 present, which rationalizes why a greater number of equivalents of H_2O_2 are needed at −30 °C. Notably, with excess H_2O_2, the Fe(III)-OOH species is formed much more slowly than at 21 °C and persists for ≫1 h (Figure S20). The acceleration observed with H_2O together with full oxidation of **1** is consistent with the acceleration of methanol/water ligand exchange and the increased opportunity for comproportionation between **2c** and **4**.

DFT Calculations. The changes in free energy over each step (Scheme 3) indicate that upon dissolving in methanol, **1** ($S = 0$) undergoes ligand exchange as observed experimentally. Ligand exchange from **2a** ($S = 0$) to form **2b** ($S = 1$) is endergonic (5.65 kcal mol^{-1}); however, heterolysis of the O−O bond yielding **4** ($S = 1$) is highly exergonic (−63.36 kcal mol^{-1}), rationalizing the absence of spectroscopic evidence for the putative intermediate **2b**. Adventitious water, as well as water that is added with H_2O_2 (50 wt % in H_2O), facilitates ligand exchange to yield $[(N4Py)Fe(II)(OH_2)]^{2+}$ (**2c**, $S = 0$) from **2a** (−0.61 kcal mol^{-1}). As reported earlier,[10] comproportionation of **2c** ($S = 0$) and **4** ($S = 1$) to form $[(N4Py)Fe(III)(OH)]^{2+}$ (**3c**, $S = \frac{1}{2}$) is also highly exergonic (−7.15 kcal mol^{-1}). $[(N4Py)Fe(III)(OCH_3)]^{2+}$ (**3a**, $S = \frac{5}{2}$), but not **3c**, is observed by EPR and Raman spectroscopy due to the exergonicity of ligand exchange in favor of the solvent methanol.[43]

The heterolysis of the O−O bond was investigated by DFT calculations. The low ($S = 0$) and high ($S = 2$) spin states of **2b** are lowest in energy and have essentially the same energy with the low-spin state ($S = 0$) only 2.9 kcal mol^{-1} higher than the $S = 2$ state. The intermediate spin ($S = 1$) state is 17.5 kcal mol^{-1} higher in Gibbs free energy. The activation energy for the heterolysis of **2b** is 1.3 kcal mol^{-1} at $S = 2$ and the reaction is exergonic (Figure S21). Unfortunately, the transition state for heterolysis at $S = 1$ was not obtained but already shows the cleavage of the O−O bond during the geometry optimization (i.e., a spontaneous process). This is consistent with its transient nature and the large exergonicity at $S = 1$ (−63.36 kcal mol^{-1}, Scheme 3). The influence of solvent and different adducts in solution on heterolysis was considered by adding CH_3OH (solvent), H_2O (residues in methanol and 50 wt % H_2O_2), and H_2O_2 (added). Seven different conditions were calculated by altering the hydrogen bond acceptor and donor to Fe(II)-OOH (Table S4). In all cases, the triplet state is the lowest in energy (Table S3) and all O−O bonds show spontaneous heterolytic cleavage upon geometry optimization (Figure 6 and Table S4). Overall, the conversion of **2b** to **4** and hydroxide is energetically downhill and has negligible activation energy. Hence, temperature will only affect the outcome of the reaction by its effect on prior ligand exchange steps, i.e., reaction of **1** rather than **2a** with H_2O_2 to form the transient **2b**. The barriers for the exchange of the methanol ligand of **2a** with H_2O_2 were calculated at all three spin states (Figure 7), which showed that the lowest barrier is observed for the $S = 2$ (high) spin state. This exchange occurs with a relatively high activation free energy (7.3 kcal mol^{-1}) and is the rate-determining step. After this exchange, the complex then moves toward CH_3OH-bound **2b** (Figure 6, bottom) for which the $S = 0$ state is again lowest in energy. Therefore,

https://doi.org/10.1021/acs.inorgchem.4c05172
Inorg. Chem. 2025, 64, 9408−9417

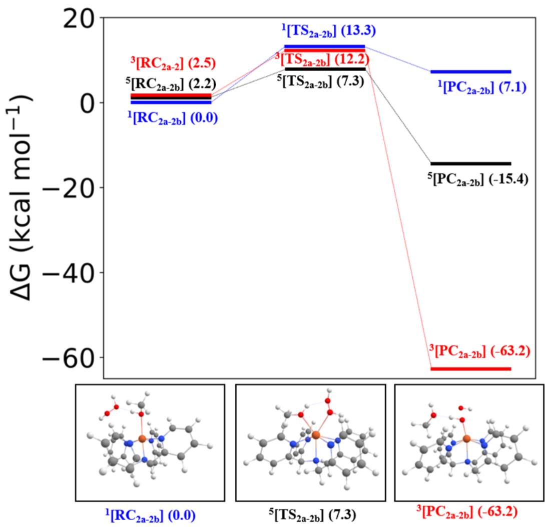

Figure 7. (Top) Energy profile (in kcal mol^{-1}) for the ligand exchange (the reaction of **2a** with H_2O_2 to form $[(N4Py)Fe(II)\text{-}(HOOH)]^{2+}$), obtained with the S12g/TZ2P//BP86-D3/TDZP level. (Bottom) Corresponding structures are shown below.

between the exchange TS and the CH_3OH-bound **2b**, a minimum energy crossing point (MECP)[51,52] must be passed.[53]

CONCLUSIONS

Generation of (L)Fe(IV)═O species from the corresponding Fe(II) complexes of the ligands TMC and bispidine in relatively high yield upon reaction with stoichiometric H_2O_2 indicated heterolysis of the O−O bond of putative (L)Fe(II)-OOH intermediates. In the present study, we show that this pathway is followed by Fe(II) complexes of the ligand N4Py and that the low yield of $[(N4Py)Fe(IV){=}O]^{2+}$ is due to competition with other reactions. The lower potency of $[(TMC)Fe(IV){=}O]^{2+}$ toward HAT, compared to that of $[(N4Py)Fe(IV){=}O]^{2+}$,[8,54] means that comproportionation of the ferrous and ferryl complexes has less impact. Although an initial O−O bond heterolysis in $[(bispidine)Fe(II)(OOH)]^{2+}$ to form $[(bispidine)Fe(IV){=}O]^{2+}$ in methanol is likely, it can be masked by homolysis of the O−O bond of $[(bispidine)\text{-}Fe(III)\text{-}OOH]^{2+}$, subsequent comproportionation between $[(bispidine)Fe(II){-}OH]^{2+}$ and Fe(IV)═O, as well as the HAT between H_2O_2 and Fe(IV)═O. We reported earlier that homolytic cleavage of the O−O bond of $[(N4Py)Fe(III)\text{-}(OOH)]^{2+}$ is not kinetically relevant[44] and in the present study, we show that comproportionation and HAT reactions of $[(N4Py)Fe(IV){=}O]^{2+}$ are important but can be slow enough in methanol to allow for the observation of the initially formed $[(N4Py)Fe(IV){=}O]^{2+}$. DFT calculations support the facile formation of $[(N4Py)Fe(IV){=}O]^{2+}$ from a putative $[(N4Py)\text{-}Fe(II)\text{-}(OOH)]^{+}$ species; however, we also show through temperature-dependent studies that ligand exchange equilibria in the Fe(II) oxidation state have a major impact on reactivity and reaction outcomes.

Despite being present in only submillimolar concentrations, the driving force for binding of CH_3CN is strong, which is driven exchange of methanol/water ligands with acetonitrile temperature is lowered. These data rationalize observations made in acetonitrile, also where a large excess of H_2O_2 is required to oxidize the complex to the Fe(III) state. Furthermore, we show that ligand exchange equilibria prior to reaction with H_2O_2 can greatly impact the temperature dependence of reactions. Finally, understanding the overall mechanism for the formation of $[(N4Py)Fe(IV){=}O]^{2+}$ by heterolytic O−O bond cleavage is important in strategies to harness the benefit of rebound reactions by $[(L)Fe(IV){=}O]^{2+}$ complexes in regenerating Fe(II) species. Controlling the relative rates of ligand exchange and comproportionation is essential in achieving a hydroxyl radical free Fe(II)/Fe(IV)═O redox cycle.

EXPERIMENTAL SECTION

$[(N4Py)Fe(II)(NCCH_3)](ClO_4)_2$ (**1**) and $[(N4Py)Fe(IV){=}O]\text{-}(PF_6)_2$ (**4**) were available from previous studies.[10,43] Solvents and chemicals were obtained from Sigma-Aldrich and used without further purification. Solvents for spectroscopy were UVASOL (Merck) grade. H_2O_2 (50 wt % in water; Aldrich Chemicals) was diluted as required in methanol.

Caution. The concentration or drying of solutions that may contain H_2O_2 should be strictly avoided. Before drying or concentration, peroxide test strips should be used to confirm that H_2O_2 is present or not, and where required, neutralization on solid $NaHSO_3$ or an alternative appropriate reducing agent should be performed. Suitable protective safeguards should be in place at all times when working with H_2O_2, due to the risk of explosion.

Caution. When working with perchlorate salts, suitable protective safeguards should be in place at all times due to the risk of explosion. Perchlorate salts should be handled in small (milligram) quantities and used only where necessary.

Physical Methods. UV/vis absorption spectra were recorded by using a Specord600 (AnalytikJena) spectrometer in quartz (1 cm path length) cuvettes. EPR spectra (X-band, 9.46 GHz) were recorded on a Bruker ECS106 or EMX Nano spectrometer at 77 K (in liquid N_2). Samples (0.5 mL) were transferred from a solution determined by UV/vis absorption spectroscopy to 3-mm-diameter quartz EPR tubes and flash-frozen in liquid N_2 immediately. Raman spectra at 355 nm are reported earlier.[45] Spectra were calibrated using acetonitrile/toluene, 50:50 (v/v), and processed (baseline correction/solvent subtraction where necessary) with Spectragryph V.1.15.

Computational Details. ADF and QUILD[55] were used to perform computational studies.[43] Geometries were optimized and frequency calculated using an unrestricted density functional BP86-D_3[56] with a triple-ζ valence plus polarization basis set on iron combined with a double-ζ valence plus polarization on all other atoms (TDZP). Single-point energy calculations were made on these geometries with the S12g spin-state consistent functional[57] in a triple-ζ valence plus double polarization (TZ2P) basis set. Free-energy corrections (ΔG) were obtained from the BP86-D_3 data and corrected for zero-point energy (ZPE); thermal and entropic corrections were made from frequency calculations at 298 K. The solvation energy was considered with the solvent methanol using the COSMO solvation model, implemented in ADF.[58] Molecular depictions for all structures were made using the IboView program (iboview.org).[59,60]

ASSOCIATED CONTENT

Supporting Information

The Supporting Information is available free of charge at https://pubs.acs.org/doi/10.1021/acs.inorgchem.4c05172.

Data for experimental section; colorimetric quantification of formaldehyde; complete electronic and Gibbs energy data; optimized structures; and Cartesian coordinates for all structures (PDF)

https://doi.org/10.1021/acs.inorgchem.4c05172
Inorg. Chem. 2025, 64, 9408−9417

AUTHOR INFORMATION

Corresponding Authors

Marcel Swart − *Institut de Quimica Computacional i Catalisi (IQCC), Departament de Quimica, Universitat de Girona, 17003 Girona, Catalonia, Spain; ICREA, Pg. Lluis Companys 23, 08010 Barcelona, Spain;* orcid.org/0000-0002-8174-8488; Email: marcel.swart@udg.edu

Wesley R. Browne − *Molecular Inorganic Chemistry, Stratingh Institute for Chemistry, Faculty of Science and Engineering, University of Groningen, 9747 AG Groningen, The Netherlands;* orcid.org/0000-0001-5063-6961; Email: w.r.browne@rug.nl

Authors

Juan Chen − *Department of Applied Chemistry, School of Science, Northwestern Polytechnical University, Xi'an, Shaanxi 710072, China;* orcid.org/0000-0002-0168-2037

Andy S. Sardjan − *Molecular Inorganic Chemistry, Stratingh Institute for Chemistry, Faculty of Science and Engineering, University of Groningen, 9747 AG Groningen, The Netherlands*

C. Maurits de Roo − *Molecular Inorganic Chemistry, Stratingh Institute for Chemistry, Faculty of Science and Engineering, University of Groningen, 9747 AG Groningen, The Netherlands;* orcid.org/0009-0004-1493-9809

Marika Di Berto Mancini − *Molecular Inorganic Chemistry, Stratingh Institute for Chemistry, Faculty of Science and Engineering, University of Groningen, 9747 AG Groningen, The Netherlands*

Apparao Draksharapu − *Molecular Inorganic Chemistry, Stratingh Institute for Chemistry, Faculty of Science and Engineering, University of Groningen, 9747 AG Groningen, The Netherlands;* Present Address: Department of Chemistry, Indian Institute of Technology Kanpur, Southern Laboratories 208A, Kanpur 208016, India; orcid.org/0000-0001-7897-3230

Davide Angelone − *Molecular Inorganic Chemistry, Stratingh Institute for Chemistry, Faculty of Science and Engineering, University of Groningen, 9747 AG Groningen, The Netherlands*

Ronald Hage − *Molecular Inorganic Chemistry, Stratingh Institute for Chemistry, Faculty of Science and Engineering, University of Groningen, 9747 AG Groningen, The Netherlands*

Complete contact information is available at:
https://pubs.acs.org/10.1021/acs.inorgchem.4c05172

Notes

The authors declare no competing financial interest.

ACKNOWLEDGMENTS

The Ubbo Emmius fund (AD), the Ministry of Education, Culture and Science of The Netherlands (Gravity Program 024.001.035, WRB), COST Action CM1305 ECOSTBio, MINECO and AEI/MCIU (PID2023-152415NB-I00, CTQ2014-59212-P, and CTQ2017-87392-P, MS), GenCat (2021SGR00487, MS), the European research council (ERC-2011-StG-279549, WRB), and the Chinese Scholarship Council (JC) are acknowledged for financial support.

REFERENCES

(1) Costas, M.; Mehn, M. P.; Jensen, M. P.; Que, L. Dioxygen Activation at Mononuclear Nonheme Iron Active Sites: Enzymes, Models, and Intermediates. *Chem. Rev.* **2004**, *104*, 939−986.

(2) Nam, W. High-Valent Iron(IV)-Oxo Complexes of Heme and Non-Heme Ligands in Oxygenation Reactions. *Acc. Chem. Res.* **2007**, *40*, 522−531.

(3) Lee, J. L.; Ross, D. L.; Barman, S. K.; Ziller, J. W.; Borovik, A. S. C-H Bond Cleavage by Bioinspired Nonheme Metal Complexes. *Inorg. Chem.* **2021**, *60*, 13759−13783.

(4) McDonald, A. R.; Que, L. High-valent nonheme iron-oxo complexes: Synthesis, structure, and spectroscopy. *Coord. Chem. Rev.* **2013**, *257*, 414−428.

(5) Lim, M. H.; Rohde, J.-U.; Stubna, A.; Bukowski, M. R.; Costas, M.; Ho, R. Y. N.; Münck, E.; Nam, W.; Que, L. An Fe ^{IV} O complex of a tetradentate tripodal nonheme ligand. *Proc. Natl. Acad. Sci. U.S.A.* **2003**, *100*, 3665−3670.

(6) Bukowski, M. R.; Koehntop, K. D.; Stubna, A.; Bominaar, E. L.; Halfen, J. A.; Münck, E.; Nam, W.; Que, L. A Thiolate-Ligated Nonheme Oxoiron(IV) Complex Relevant to Cytochrome P450. *Science* **2005**, *310*, 1000−1002.

(7) Rohde, J.-U.; In, J.-H.; Lim, M. H.; Brennessel, W. W.; Bukowski, M. R.; Stubna, A.; Münck, E.; Nam, W.; Que, L. Crystallographic and Spectroscopic Characterization of a Nonheme Fe(IV)=O Complex. *Science* **2003**, *299*, 1037−1039.

(8) Kaizer, J.; Klinker, E. J.; Oh, N. Y.; Rohde, J.-U.; Song, W. J.; Stubna, A.; Kim, J.; Münck, E.; Nam, W.; Que, L. Nonheme Fe ^{IV}O Complexes That Can Oxidize the C-H Bonds of Cyclohexane at Room Temperature. *J. Am. Chem. Soc.* **2004**, *126*, 472−473.

(9) Kumar, D.; Hirao, H.; Que, L.; Shaik, S. Theoretical Investigation of C-H Hydroxylation by (N4Py)Fe $^{IV}O^{2+}$: An Oxidant More Powerful than P450? *J. Am. Chem. Soc.* **2005**, *127*, 8026−8027.

(10) Draksharapu, A.; Angelone, D.; Quesne, M. G.; Padamati, S. K.; Gómez, L.; Hage, R.; Costas, M.; Browne, W. R.; de Visser, S. P. Identification and Spectroscopic Characterization of Nonheme Iron(III) Hypochlorite Intermediates. *Angew. Chem., Int. Ed.* **2015**, *54*, 4357−4361.

(11) Sastri, C. V.; Sook Seo, M.; Joo Park, M.; Mook Kim, K.; Nam, W. Formation, stability, and reactivity of a mononuclear nonheme oxoiron(iv) complex in aqueous solution. *Chem. Commun.* **2005**, 1405.

(12) Kaizer, J.; Costas, M.; Que, L. A Dramatic Push Effect on the Homolysis of Fe ^{III} (OOR) Intermediates To Form Non-Heme Fe ^{IV} =O Complexes. *Angew. Chem., Int. Ed.* **2003**, *42*, 3671−3673.

(13) Bercy, R.; Rebilly, J.; Herrero, C.; Guillot, R.; Maisonneuve, H.; Banse, F. Beneficial Effect of Acetic Acid on the Formation of Fe ^{III} (OOH) Species and on the Catalytic Activity of Bioinspired Nonheme Fe ^{II} Complexes. *Eur. J. Inorg. Chem.* **2023**, *26*, No. e202300236.

(14) Bohn, A.; Chinaux-Chaix, C.; Cheaib, K.; Guillot, R.; Herrero, C.; Sénéchal-David, K.; Rebilly, J.-N.; Banse, F. Base-controlled mechanistic divergence between iron(IV)oxo and iron(III)-hydroperoxo in the H $_2$ O $_2$ activation by a nonheme iron(II) complex. *Dalton Trans.* **2019**, *48*, 17045−17051.

(15) Rebilly, J.-N.; Herrero, C.; Sénéchal-David, K.; Guillot, R.; Inceoglu, T.; Maisonneuve, H.; Banse, F. Second-sphere effects on H_2O_2 activation by non-heme Fe^{II} complexes: role of a phenol group in the $[H_2O_2]$-dependent accumulation of $Fe^{IV}O$ vs. $Fe^{III}OOH$. *Chem. Sci.* **2021**, *12*, 15691−15699.

(16) Kripli, B.; Sólyom, B.; Speier, G.; Kaizer, J. Stability and Catalase-Like Activity of a Mononuclear Non-Heme Oxoiron(IV) Complex in Aqueous Solution. *Molecules* **2019**, *24*, 3236.

(17) Lubben, M.; Meetsma, A.; Wilkinson, E. C.; Feringa, B.; Que, L. Nonheme Iron Centers in Oxygen Activation: Characterization of an Iron(III) Hydroperoxide Intermediate. *Angew. Chem., Int. Ed.* **1995**, *34*, 1512−1514.

(18) Roelfes, G.; Lubben, M.; Hage, R.; Que, L., Jr.; Feringa, B. L. Catalytic Oxidation with a Non-Heme Iron Complex That Generates

a Low-Spin $Fe^{III}OOH$ Intermediate. *Chem. - Eur. J.* **2000**, *6*, 2152−2159.

(19) Sam, J. W.; Tang, X.-J.; Peisach, J. Electrospray Mass Spectrometry of Iron Bleomycin: Demonstration That Activated Bleomycin Is a Ferric Peroxide Complex. *J. Am. Chem. Soc.* **1994**, *116*, 5250−5256.

(20) Oloo, W. N.; Fielding, A. J.; Que, L. Rate-Determining Water-Assisted O-O Bond Cleavage of an Fe^{III} -OOH Intermediate in a Bio-inspired Nonheme Iron-Catalyzed Oxidation. *J. Am. Chem. Soc.* **2013**, *135*, 6438−6441.

(21) Mondal, B.; Neese, F.; Bill, E.; Ye, S. Electronic Structure Contributions of Non-Heme Oxo-Iron(V) Complexes to the Reactivity. *J. Am. Chem. Soc.* **2018**, *140*, 9531−9544.

(22) Prat, I.; Mathieson, J. S.; Güell, M.; Ribas, X.; Luis, J. M.; Cronin, L.; Costas, M. Observation of Fe(V)═O using variable-temperature mass spectrometry and its enzyme-like C-H and C = C oxidation reactions. *Nat. Chem.* **2011**, *3*, 788−793.

(23) Lyakin, O. Y.; Bryliakov, K. P.; Britovsek, G. J. P.; Talsi, E. P. EPR Spectroscopic Trapping of the Active Species of Nonheme Iron-Catalyzed Oxidation. *J. Am. Chem. Soc.* **2009**, *131*, 10798−10799.

(24) Lyakin, O. Y.; Ottenbacher, R. V.; Bryliakov, K. P.; Talsi, E. P. Asymmetric Epoxidations with H_2 O_2 on Fe and Mn Aminopyridine Catalysts: Probing the Nature of Active Species by Combined Electron Paramagnetic Resonance and Enantioselectivity Study. *ACS Catal.* **2012**, *2*, 1196−1202.

(25) Oloo, W. N.; Meier, K. K.; Wang, Y.; Shaik, S.; Münck, E.; Que, L. Identification of a low-spin acylperoxoiron(III) intermediate in bio-inspired non-heme iron-catalysed oxidations. *Nat. Commun.* **2014**, *5*, No. 3046.

(26) Serrano-Plana, J.; Oloo, W. N.; Acosta-Rueda, L.; Meier, K. K.; Verdejo, B.; García-España, E.; Basallote, M. G.; Münck, E.; Que, L.; Company, A.; Costas, M. Trapping a Highly Reactive Nonheme Iron Intermediate That Oxygenates Strong CH Bonds with Stereo-retention. *J. Am. Chem. Soc.* **2015**, *137*, 15833−15842.

(27) Bukowski, M. R.; Zhu, S.; Koehntop, K. D.; Brennessel, W. W.; Que, L. Characterization of an Fe^{III}-OOH species and its decomposition product in a bleomycin model system. *J. Biol. Inorg. Chem.* **2004**, *9*, 39−48.

(28) Deville, C.; Finsel, M.; De Sousa, D. P.; Szafranowska, B.; Behnken, J.; Svane, S.; Bond, A. D.; Seidler-Egdal, R. K.; McKenzie, C. J. Too Many Cooks Spoil the BrothVariable Potencies of Oxidizing Mn Complexes of a Hexadentate Carboxylato Ligand. *Eur. J. Inorg. Chem.* **2015**, *2015*, 3543−3549.

(29) Vad, M. S.; Lennartson, A.; Nielsen, A.; Harmer, J.; McGrady, J. E.; Frandsen, C.; Mørup, S.; McKenzie, C. J. An aqueous non-heme Fe(IV)oxo complex with a basic group in the second coordination sphere. *Chem. Commun.* **2012**, *48*, No. 10880.

(30) De Sousa, D. P.; Miller, C. J.; Chang, Y.; Waite, T. D.; McKenzie, C. J. Electrochemically Generated Scis -Carboxylato-Coordinated Iron(IV) Oxo Acid-Base Congeners as Promiscuous Oxidants of Water Pollutants. *Inorg. Chem.* **2017**, *56*, 14936−14947.

(31) Piquette, M. C.; Kryatov, S. V.; Rybak-Akimova, E. V. Kinetic Studies on the Oxoiron(IV) Complex with Tetradentate Amino-pyridine Ligand PDP*: Restoration of Catalytic Activity by Reduction with H_2O_2. *Inorg. Chem.* **2019**, *58*, 13382−13393.

(32) Pangia, T. M.; Davies, C. G.; Prendergast, J. R.; Gordon, J. B.; Siegler, M. A.; Jameson, G. N. L.; Goldberg, D. P. Observation of Radical Rebound in a Mononuclear Nonheme Iron Model Complex. *J. Am. Chem. Soc.* **2018**, *140*, 4191−4194.

(33) Bang, S.; Park, S.; Lee, Y.; Hong, S.; Cho, K.; Nam, W. Demonstration of the Heterolytic O-O Bond Cleavage of Putative Nonheme Iron(II)OOH(R) Complexes for Fenton and Enzymatic Reactions. *Angew. Chem., Int. Ed.* **2014**, *53*, 7843−7847.

(34) Lee, Y.-M.; Bang, S.; Kim, Y. M.; Cho, J.; Hong, S.; Nomura, T.; Ogura, T.; Troeppner, O.; Ivanović-Burmazović, I.; Sarangi, R.; Fukuzumi, S.; Nam, W. A mononuclear nonheme iron(III)-peroxo complex binding redox-inactive metal ions. *Chem. Sci.* **2013**, *4*, 3917.

(35) Li, F.; England, J.; Que, L. Near-Stoichiometric Conversion of H_2O_2 to Fe^{IV} = O at a Nonheme Iron(II) Center. Insights into the O-O Bond Cleavage Step. *J. Am. Chem. Soc.* **2010**, *132*, 2134−2135.

(36) Bautz, J.; Bukowski, M. R.; Kerscher, M.; Stubna, A.; Comba, P.; Lienke, A.; Münck, E.; Que, L. Formation of an Aqueous Oxoiron(IV) Complex at pH 2−6 from a Nonheme Iron(II) Complex and H_2 O_2. *Angew. Chem., Int. Ed.* **2006**, *45*, 5681−5684.

(37) Hirao, H.; Li, F.; Que, L.; Morokuma, K. Theoretical Study of the Mechanism of Oxoiron(IV) Formation from H_2O_2 and a Nonheme Iron(II) Complex: O-O Cleavage Involving Proton-Coupled Electron Transfer. *Inorg. Chem.* **2011**, *50*, 6637−6648.

(38) Cheaib, K.; Mubarak, M. Q. E.; Sénéchal-David, K.; Herrero, C.; Guillot, R.; Clémancey, M.; Latour, J.; de Visser, S. P.; Mahy, J.; Banse, F.; Avenier, F. Selective Formation of an $Fe^{IV}O$ or an $Fe^{III}OOH$ Intermediate From Iron(II) and H_2O_2: Controlled Heterolytic versus Homolytic Oxygen-Oxygen Bond Cleavage by the Second Coordination Sphere. *Angew. Chem., Int. Ed.* **2019**, *58*, 854−858.

(39) Bohn, A.; Sénéchal-David, K.; Rebilly, J.; Herrero, C.; Leibl, W.; Anxolabéhère-Mallart, E.; Banse, F.; Heterolytic, O. Heterolytic O-O Bond Cleavage Upon Single Electron Transfer to a Nonheme Fe(III)-OOH Complex. *Chem. - Eur. J.* **2022**, *28*, No. e202201600.

(40) Braymer, J. J.; O'Neill, K. P.; Rohde, J.; Lim, M. H. The Reaction of a High-Valent Nonheme Oxoiron(IV) Intermediate with Hydrogen Peroxide. *Angew. Chem., Int. Ed.* **2012**, *51*, 5376−5380.

(41) Drummond, M. J.; Ford, C. L.; Gray, D. L.; Popescu, C. V.; Fout, A. R. Radical Rebound Hydroxylation Versus H-Atom Transfer in Non-Heme Iron(III)-Hydroxo Complexes: Reactivity and Structural Differentiation. *J. Am. Chem. Soc.* **2019**, *141*, 6639−6650.

(42) Roelfes, G.; Vrajmasu, V.; Chen, K.; Ho, R. Y. N.; Rohde, J.-U.; Zondervan, C.; La Crois, R. M.; Schudde, E. P.; Lutz, M.; Spek, A. L.; Hage, R.; Feringa, B. L.; Münck, E.; Que, L. End-On and Side-On Peroxo Derivatives of Non-Heme Iron Complexes with Pentadentate Ligands: Models for Putative Intermediates in Biological Iron/Dioxygen Chemistry. *Inorg. Chem.* **2003**, *42*, 2639−2653.

(43) Chen, J.; Draksharapu, A.; Angelone, D.; Unjaroen, D.; Padamati, S. K.; Hage, R.; Swart, M.; Duboc, C.; Browne, W. R. H_2O_2 Oxidation by Fe^{III}-OOH Intermediates and Its Effect on Catalytic Efficiency. *ACS Catal.* **2018**, *8*, 9665−9674.

(44) Maurits De Roo, C.; Sardjan, A. S.; Postmus, R.; Swart, M.; Hage, R.; Browne, W. R. Reaction of (N4Py)Fe with H_2O_2 and the relevance of its Fe(IV)═O species during and after H_2 O_2 disproportionation. *ChemCatChem* **2024**, *16*, No. e202301594.

(45) Draksharapu, A.; Li, Q.; Logtenberg, H.; Van Den Berg, T. A.; Meetsma, A.; Killeen, J. S.; Feringa, B. L.; Hage, R.; Roelfes, G.; Browne, W. R. Ligand Exchange and Spin State Equilibria of Fe^{II}(N4Py) and Related Complexes in Aqueous Media. *Inorg. Chem.* **2012**, *51*, 900−913.

(46) Bukowski, M. R.; Comba, P.; Limberg, C.; Merz, M.; Que, L.; Wistuba, T. Bispidine Ligand Effects on Iron/Hydrogen Peroxide Chemistry. *Angew. Chem., Int. Ed.* **2004**, *43*, 1283−1287.

(47) Liu, L. V.; Hong, S.; Cho, J.; Nam, W.; Solomon, E. I. Comparison of High-Spin and Low-Spin Nonheme Fe^{III} -OOH Complexes in O-O Bond Homolysis and H-Atom Abstraction Reactivities. *J. Am. Chem. Soc.* **2013**, *135*, 3286−3299.

(48) Oh, N. Y.; Suh, Y.; Park, M. J.; Seo, M. S.; Kim, J.; Nam, W. Mechanistic Insight into Alcohol Oxidation by High-Valent Iron-Oxo Complexes of Heme and Nonheme Ligands. *Angew. Chem.* **2005**, *117*, 4307−4311.

(49) Chen, J.; Draksharapu, A.; Harvey, E.; Rasheed, W.; Que, L.; Browne, W. R. Direct photochemical activation of non-heme Fe(IV)O complexes. *Chem. Commun.* **2017**, *53*, 12357−12360.

(50) < 20%, i.e. below the limit of detection in the present study[61]

(51) Harvey, J. N.; Aschi, M.; Schwarz, H.; Koch, W. The singlet and triplet states of phenyl cation. A hybrid approach for locating minimum energy crossing points between non-interacting potential energy surfaces. *Theor. Chem. Acc.* **1998**, *99*, 95−99.

(52) Harvey, J. N.; Aschi, M. Spin-forbidden dehydrogenation of methoxy cation: a statistical view. *Phys. Chem. Chem. Phys.* **1999**, *1*, 5555−5563.
(53) Using a rapid method for minimization of structures (BP86-D_3/TDZP) followed by single-point calculations with a spin state, consistent DFA (S12g/TZ2P) to determine MECPs is counter-productive. The structures where $S = 1$ and $S = 2$ spin states have the same energy are not obtained with the S12g/TZ2P//BP86-D_3/TDZP approach, as it leads to the structure where the BP86-D3 energies for $S = 1$ and $S = 2$ are equal.
(54) Sastri, C. V.; Lee, J.; Oh, K.; Lee, Y. J.; Lee, J.; Jackson, T. A.; Ray, K.; Hirao, H.; Shin, W.; Halfen, J. A.; Kim, J.; Que, L.; Shaik, S.; Nam, W. Axial ligand tuning of a nonheme iron(IV)-oxo unit for hydrogen atom abstraction. *Proc. Natl. Acad. Sci. U.S.A.* **2007**, *104*, 19181−19186.
(55) Swart, M.; Bickelhaupt, F. M. QUILD: QUantum-regions interconnected by local descriptions. *J. Comput. Chem.* **2008**, *29*, 724−734.
(56) Grimme, S.; Antony, J.; Ehrlich, S.; Krieg, H. A consistent and accurate Sab initio parametrization of density functional dispersion correction (DFT-D) for the 94 elements H-Pu. *J. Chem. Phys.* **2010**, *132*, No. 154104.
(57) Swart, M.; Gruden, M. Spinning around in Transition-Metal Chemistry. *Acc. Chem. Res.* **2016**, *49*, 2690−2697.
(58) Swart, M.; Rösler, E.; Bickelhaupt, F. M. Proton Affinities in Water of Maingroup-Element Hydrides - Effects of Hydration and Methyl Substitution. *Eur. J. Inorg. Chem.* **2007**, *2007*, 3646−3654.
(59) Knizia, G.; Klein, J. E. M. N. Electron Flow in Reaction MechanismsRevealed from First Principles. *Angew. Chem., Int. Ed.* **2015**, *54*, 5518−5522.
(60) Knizia, G. Intrinsic Atomic Orbitals: An Unbiased Bridge between Quantum Theory and Chemical Concepts. *J. Chem. Theory Comput.* **2013**, *9*, 4834−4843.
(61) Nash, T. The colorimetric estimation of formaldehyde by means of the Hantzsch reaction. *Biochem. J.* **1953**, *55*, 416−421.

https://doi.org/10.1021/acs.inorgchem.4c05172
Inorg. Chem. 2025, 64, 9408−9417